The Astrophysical Journal, 626:L121–L124, 2005 June 20
© 2005. The American Astronomical Society. All rights reserved. Printed in U.S.A.

FIRST SOFT X-RAY OBSERVATIONS OF GLOBAL CORONAL WAVES WITH THE *GOES* SOLAR X-RAY IMAGER

A. Warmuth, G. Mann, and H. Aurass
Astrophysikalisches Institut Potsdam, An der Sternwarte 16, D-14482 Potsdam, Germany; awarmuth@aip.de
Received 2005 February 22; accepted 2005 May 10; published 2005 May 31

ABSTRACT

We present the first observations of global coronal waves obtained with the Solar X-Ray Imager (SXI) aboard the *GOES-12* satellite. Focusing on six events, the basic morphological and kinematic characteristics of the waves observed in soft X-rays are derived. Taking advantage of SXI's high temporal cadence and comparing the wave signatures with extreme-UV, Hα, and He I data, we prove that both chromospheric and coronal signatures of waves can be created by a single decelerating disturbance, presumably a large-amplitude simple wave or shock. We stress that SXI is a very useful tool for studying coronal waves and other transients because of its high cadence and duty cycle.

Subject headings: Sun: activity — Sun: chromosphere — Sun: corona — Sun: X-rays, gamma rays — waves

1. INTRODUCTION

Since 1997, the EIT instrument aboard the *Solar and Heliospheric Observatory* (*SOHO*; Delaboudinière et al. 1995) has recorded a large number of globally propagating coronal waves (Thompson et al. 1998) in the extreme-ultraviolet (EUV). Such waves were expected from Hα observations of wavelike signatures called Moreton waves (see, e.g., Moreton 1960). In the "sweeping skirt" scenario (e.g., Uchida 1974), they represent the chromospheric ground tracks of coronal fast-mode wave fronts, which can also generate metric type II radio bursts (e.g., Mann 1995a) if they are shocked or large-amplitude simple waves (cf. Mann 1995b). However, the identification of "EIT waves" as the coronal counterpart to Moreton waves is still being debated, since they are 2–3 times slower than Moreton waves, appear much more frequently, and have a more diffuse and irregular morphology (see, e.g., Klassen et al. 2000).

Some EIT waves displays sharp wave fronts that are reminiscent of Moreton waves. These "brow waves" (Gopalswamy et al. 2000) are always observed close to the source active region. For several events it was shown that the brow waves closely matched with the associated Moreton wave fronts (Thompson et al. 2000; Khan & Aurass 2002; Warmuth et al. 2004a). Thus, at least the brow waves seem to be the coronal counterpart of Moreton waves. Warmuth et al. (2001, 2004a, 2004b) have argued that in the events where there is a prominent Moreton wave, even the more common diffuse EIT wave features can be created by the same physical disturbance, since the observed deceleration of the waves resolves the "velocity discrepancy" mentioned above. Other authors (e.g., Okamoto et al. 2004) have presented events in which it is claimed that the two phenomena are distinct. The main reason for this controversy is the low image cadence of EIT (≈12 minutes), which does not allow a precise measurement of the kinematics of the waves. Thus, other data sources must be considered.

Vršnak et al. (2002) have studied wave signatures observed in He I (10830 Å) filtergrams. In He I, the waves can be traced to larger distances than in Hα, while at the same time the temporal cadence is significantly better than for EIT. For one event it was shown that Hα, He I, and EIT wave fronts can indeed be explained by a common disturbance. However, because of the complicated line formation mechanism of He I, the interpretation of the data is complicated, and moreover, the He I signatures are diffuse (see also Gilbert et al. 2004).

In contrast to He I data, soft X-ray (SXR) observations offer the opportunity to observe the coronal waves directly. A few waves were observed with the *Yohkoh* Soft X-Ray Telescope (SXT; Tsuneta et al 1991), and it was shown that they match the kinematic curves of the associated Moreton waves (Khan & Aurass 2002; Narukage et al. 2002). However, because of the small field of view in SXT's flaring mode, these waves could not be traced far enough in order to study their relation with global EIT waves.

Currently, solar SXR imaging is solely provided by the Solar X-Ray Imager (SXI) aboard the *GOES-12* satellite. SXI was designed as an operational instrument with the primary goal of providing data for space weather forecasting. It provides full-disk coverage and a superior time cadence as compared with EIT, and we have succeeded in detecting coronal waves with SXI. In this Letter, we report on the basic characteristics of these "SXI waves," using six events from 2003 October and November, when the Sun was extremely active. In addition, we study the relation of these waves to signatures in other frequency ranges and show that indeed all observational features can be explained by a common disturbance.

2. OBSERVATIONS

SXI is a grazing-incidence telescope (Lemen et al. 2004) that provides full-disk solar images (with a resolution of 5″ pixel^{-1}) using various analysis filters. For observing coronal structures, long-exposure (3 s) images are used that are acquired in the OPEN configuration without any filter (sensitive to temperatures of ≈3 MK), as well as with the thin and medium polyimide filters (PTHN and PMED; covering temperatures of ≈4 and ≈5 MK, respectively). These filters have a broad temperature response of about ±2 MK FWHM.

Between 2003 October 29 and November 4, OPEN data were available at a cadence of 4 minutes (8 minutes for PTHN and PMED). In this period the active regions (ARs) 0486 and 0488 (indicated in the OPEN context image in Fig. 1) produced numerous energetic flares and coronal mass ejections (CMEs). The three SXI channels were checked for wave signatures by examining difference and running-difference images. In the OPEN and in the PTHN images, waves were detected for all six events, while only four events showed up in the PMED data (where the fronts were only marginally visible). All waves were also observed by EIT. The events are listed in Table 1, together with their label, AR number, the starting and peak

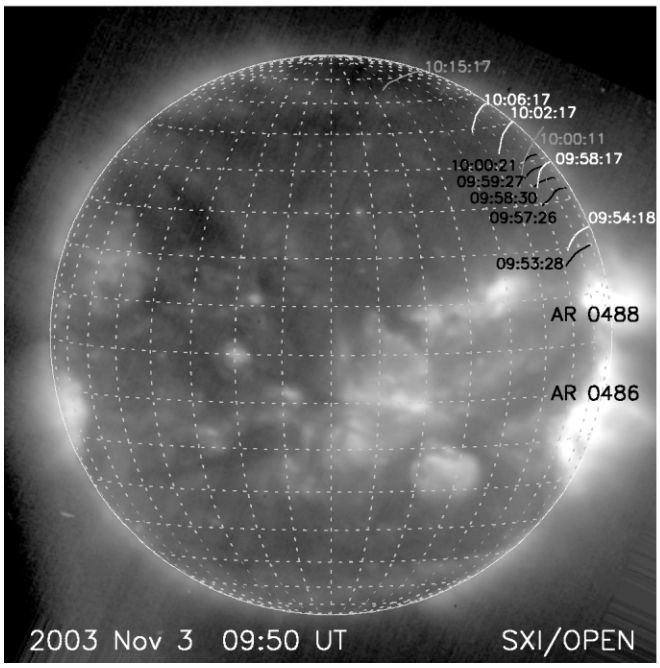

FIG. 1.—SXI OPEN context image of the event E5 (2003 November 3) just before flare and wave onset. Overplotted are SXI (*white*), EIT (*gray*), and Hα wave fronts (*black*). The times of the wave fronts are given in UT. Also indicated are ARs 0486 and 0488.

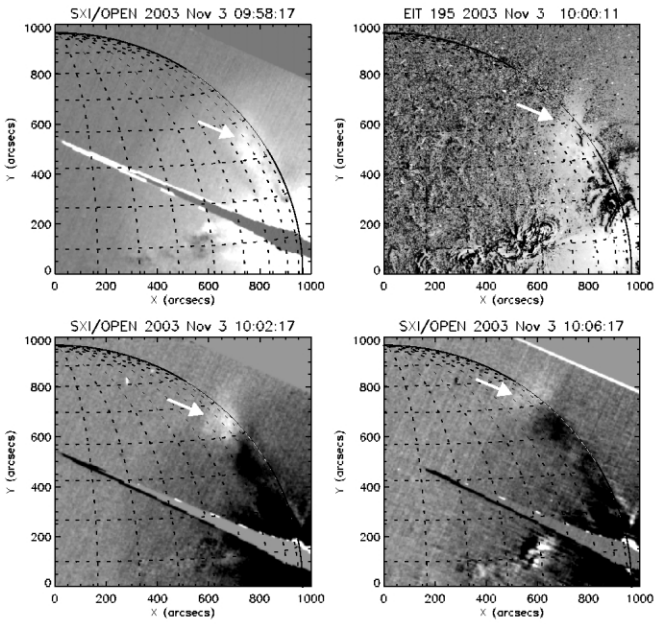

FIG. 2.—Propagation of the coronal wave (*indicated by arrows*) of event E5 as shown by SXI OPEN running-difference images. The EIT 195 Å difference image (*top right*) shows that the morphology of the wave front is similar in SXRs and EUV. The inclined linear feature in the SXI images is due to overexposure from the flare.

time of the associated *GOES* flare and its class, and the association with CMEs and metric type II bursts, as well as the most important kinematic parameters. With the exception of E2, all events were associated with strong or impulsive flares, as well as with CMEs (determined from *SOHO* LASCO images; see Brueckner et al. 1995) and type II bursts (as given by the National Geophysical Data Center catalog).[1]

3. DISCUSSION

Figure 2 shows OPEN running-difference images of the best-defined wave event, E5, associated with an X3.9 flare and a fast CME on 2003 November 3. The wave front is clearly visible as an area of increased emission propagating away from AR 0488. Note that the front also extends above the solar limb: it reaches heights of up to ≈100 Mm, while the bulk of the emission increase resides below ≈50 Mm. The EIT frame included in Figure 2 shows that the EUV and SXR signatures are very similar. The average increase in SXR emission in the OPEN wave fronts was about 10% with respect to the quiet Sun, while the maximum increase over small areas was up to 50%. The same values were found for the single PTHN wave front in this event, while the contrast was twice as high in the corresponding EIT front. The broadly comparable brightness increase over the range from 1.5 to 4 MK implies that the coronal disturbance must be compressive and cannot solely be due to temperature changes.

The SXI waves observed in the other events generally had the same characteristics, though in some cases they were difficult to observe (especially near the source AR) because of a halo of scattered light around the flare site. Interestingly, the events coming from the southern AR 0486 consisted of two fronts heading both north and south, while the waves emanating from AR 0488 all propagated north. This implies that the wave-producing AR has an important influence on the launch and the geometry of a coronal wave, presumably due to its magnetic topology.

In order to determine the relation of the SXI waves to the chromospheric signatures, we have checked the events for wave signatures in Hα and He I (using data from the solar observatories Kanzelhöhe, Big Bear and Mauna Loa; see Warmuth et al. 2004a and references therein for a description of the instruments). Hα waves were found in E1, E4, E5, and E6, while weak He I signatures were present in E1. Again, the Hα waves of AR 0486 are simultaneously heading northward and southward, which is the first time that this has been observed for Moreton waves. For E5, the wave fronts are shown in Figure 1.

[1] See ftp://ftp.ngdc.noaa.gov/STP/SOLAR_DATA.

TABLE 1
CORONAL WAVES OBSERVED BY SXI AND ASSOCIATED EVENTS

Label/Date	AR	Start (UT)	Max (UT)	Class	CME?	Type II?	$v_{1,\mathrm{SXI}}$ (km s^{-1})	$v_{f,\mathrm{SXI}}$ (km s^{-1})	$\bar{v}_{\mathrm{EIT}}$ (km s^{-1})	$\bar{a}_{\mathrm{cb}}$ (m s^{-2})
E1: 2003 Oct 29	0486	20:37	20:49	X10.0	Yes	Yes	317	317	...	−146
E2: 2003 Nov 2	0488	11:24	11:30	C2.9	No	No	562	283	209	−145
E3: 2003 Nov 2	0486	17:03	17:25	X8.3	Yes	Yes	383	241	290	−111
E4: 2003 Nov 3	0488	01:09	01:30	X2.7	Yes	Yes	424	317	195	−137
E5: 2003 Nov 3	0488	09:43	09:55	X3.9	Yes	Yes	740	351	420	−338
E6: 2003 Nov 4	0486	19:29	19:53	X28+	Yes	Yes	461	425	...	−1441

The distances $r(t)$ of the leading edges from the center of the flare were measured along 10 great circles (see Warmuth et al. 2004a) for all SXI, EIT, Hα, and He I wave fronts. The result is shown in Figure 3, where the numbers of fronts in the various spectral bands are also given (for brevity, only the northbound waves are shown for AR 0486). Hard X-ray (HXR) light curves (25–50 keV; plotted in arbitrary units) from *RHESSI* (Lin et al. 2002) are included at the bottom of each graph to show the context of the associated flares (for E2 and E6, the derivative of the flux in the 3–25 keV *GOES* channel is shown as a proxy for the HXR emission). Most waves are apparently launched near the impulsive energy release phase, while E3 and E5 seem to start up to 10 minutes earlier. A detailed study of the association of coronal waves with flares and CMEs is currently in preparation.

Figure 3 shows that the wave fronts are consistent with a single physical disturbance causing the different signatures, that is, they agree with a common kinematic curve. This confirms the findings of Warmuth et al. (2004a). Some basic kinematic parameters of the disturbances are listed in Table 1 (again, only the northbound waves are included): the starting and final speed of the SXI waves, $v_{1,\mathrm{SXI}}$ and $v_{f,\mathrm{SXI}}$, the mean EIT wave speed $\bar{v}_{\mathrm{EIT}}$, and the mean acceleration obtained when combining the different measurements, $\bar{a}_{\mathrm{cb}}$. Speeds are given in kilometers per second, accelerations in meters per second per second. Averaged over all events, we find a mean deceleration of $\langle \bar{a}_{\mathrm{cb}} \rangle = -330 \pm 430$ m s^{-2} [as given by a second-degree polynomial fit to $r(t)$] and a mean linear speed of $\langle \bar{v}_{\mathrm{cb}} \rangle = 420 \pm 190$ km s^{-1}. These values closely correspond to the results of Warmuth et al. (2004a), which means that we are studying the same class of events.

Let us examine the best-defined event, E5, in more detail. Here the SXI fronts overlap both the observed range of the Hα wave and the EIT wave. The SXI wave closely agrees with *both* the Moreton wave (which can be observed only comparatively close to the AR) *and* the more distant and diffuse EIT wave (see Fig. 3). This proves the claim of Warmuth et al. (2004a) that the more distant, diffuse EIT waves are generated by the same disturbance that is responsible for the sharp signatures near the AR. Moreover, we found no evidence of a second wave front in the SXI data, which should be expected if there were two physically distinct disturbances present in a single event (cf. the model of Chen et al. 2002).

The role of SXI wave signatures as a missing link between Moreton and EIT waves is also reflected by the kinematic parameters derived from the particular spectral regimes. For example, the mean decelerations were $\langle \bar{a}_{\mathrm{H}\alpha} \rangle = -600 \pm 560$ m s^{-2} for the Moreton waves, $\langle \bar{a}_{\mathrm{SXI}} \rangle = -270 \pm 300$ m s^{-2} for the SXI waves, and $\langle \bar{a}_{\mathrm{EIT}} \rangle = -190 \pm 70$ m s^{-2} for the EIT waves. The mean linear velocities were $\langle \bar{v}_{\mathrm{H}\alpha} \rangle = 660 \pm 440$ km s^{-1}, $\langle \bar{v}_{\mathrm{SXI}} \rangle = 380 \pm 100$ km s^{-1}, and $\langle \bar{v}_{\mathrm{EIT}} \rangle = 320 \pm 120$ km s^{-1}. The parameters derived from SXI lie between the two extremes obtained from Hα and EIT data, which means that SXI observations sample *both* regimes: the vicinity of the AR, where the wave is fast and strongly decelerating, and the more remote areas of the quiet corona, where the disturbance has a lower and nearly constant speed.

This behavior, which was present in all events, combined with the decrease of the waves' intensity, is typical of a large-amplitude magnetohydrodynamic simple wave (cf. Mann 1995b). Because of the nonlinearities, the speed of a fast-mode (compressive) simple wave monotonically increases with the local density compression of the wave. Thus, the leading edge propagates faster than the trailing edge, resulting in wave steepening, which finally leads to the formation of a shock. Since the trailing edge has a small amplitude, it moves with the linear fast magnetosonic speed v_{ms}, whereas the leading edge propagates supermagnetosonically at $v_{\mathrm{lead}} = M_{\mathrm{ms}} v_{\mathrm{ms}}$, where $M_{\mathrm{ms}} > 1$ is the magnetosonic Mach number. The linear fast magnetosonic speed (valid for waves propagating perpendicular to the magnetic field lines) is given by $v_{\mathrm{ms}} = (v_{\mathrm{A}}^2 + c_s^2)^{1/2}$, where

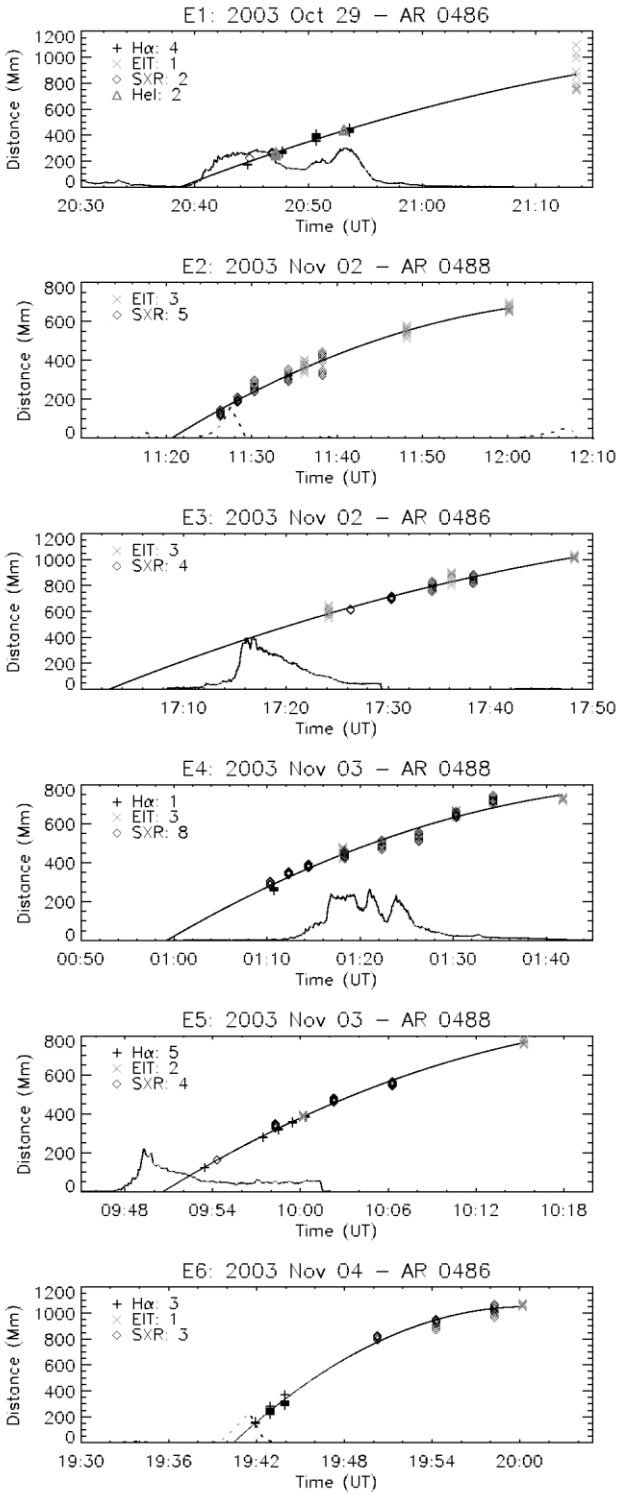

FIG. 3.—Kinematics of the coronal waves. Distances $r(t)$ (in Mm) are plotted together with second-degree polynomial fits. Also included are HXR light curves of the associated flares.

v_A is the Alfvén speed and c_s is the sound speed. The fact that $v_{lead} > v_{trail}$ also causes a broadening of the waves' profile, which is observed. Combined with the geometric expansion, this leads to a drop in the perturbation amplitude, which also means that the disturbance will slow down and may finally decay to a linear wave propagating at v_{ms}.

We stress that the waves discussed in this Letter all decelerated to comparable speeds, as given, for example, by the mean EIT speed $\langle \bar{v}_{EIT} \rangle = 320 \pm 120$ km s^{-1} (cf. Table 1). This agrees very closely with the value of $\langle \bar{v}_{H\alpha} \rangle = 311 \pm 84$ km s^{-1} found by Warmuth et al. (2004a). These velocities thus do not reflect the properties connected to an individual event (e.g., the speed of ejected matter in an eruptive scenario), but rather the characteristic speed of the ambient medium, that is, v_{ms}. This supports the notion that in the regions far from the source AR, the disturbances are fast-mode waves.

However, EIT waves show a broad range of morphological characteristics and velocities (cf. Biesecker et al. 2002), which suggests that they may be caused by several different processes. Many EIT "waves" may not be waves at all, but signatures of eruptive processes or coronal restructuring (cf. Delannée 2000; Zhukov & Auchère 2004). An example for this might be the transient event starting at 08:30 on 2003 November 2 that was observed by SXI and EIT. This event was more irregular than those discussed above, had no associated flares, CMEs or radio bursts, and had a speed of only ≈100 km s^{-1}.

The fact that probably a considerable fraction of coronal transients are not really waves at all poses a problem for their use as tools for deriving ambient coronal parameters ("coronal seismology"; e.g., Warmuth & Mann 2005), which requires that the disturbances be MHD waves. Based on our results, a coronal transient can be considered a wave if the following characteristics are present: a single front seen in emission in SXRs and EUV with a relatively smooth shape close to the source AR, a decelerating motion with a mean deceleration of a few hundred meters per second per second, and speeds around 300 km s^{-1} at large distances from the AR. The association with strong or very impulsive flares, fast CMEs, and metric type II bursts also seems to be common for these wave events, though these are perhaps not necessary conditions, as shown by their absence in E2.

Regarding terminology, we propose a more exact usage of terms. "Coronal wave" should exclusively be used for moving features that are most likely waves (including large-amplitude simple waves and shocks), according to the characteristics given above. "Coronal wave" should be considered the general term referring to the physical disturbance, while "EIT wave," etc., can be used when discussing observations from the respective channels. For moving coronal features whose physical nature has yet to be determined, more general terms such as "coronal transient" or "moving coronal disturbance" can be used.

We conclude that a coronal transient that is observable with EIT will generally also be imaged by SXI. The SXI observations presented here are consistent with the scenario of a large-amplitude simple wave that generates all signatures in the various spectral ranges. SXI is ideally suited for a consistent study of how initially supermagnetosonic coronal waves decay to ordinary fast-mode waves. The high cadence of SXI also allows for a better kinematic characterization of the waves, even when supplementary data such as Hα images are not available or when the event is too weak to produce chromospheric signatures. Note that after the loss of the OPEN filter configuration on 2003 November 5, long-exposure PTHN images are now available at a cadence of 2 minutes. Given the high duty cycle of SXI, this means that over the next few years an event sample of hundreds of kinematically resolved coronal transients will be compiled. This large data set will hopefully allow us to solve some of the long-standing issues regarding coronal waves and other transients, the most important one being the question of how these disturbances are initially launched.

The work of A. W. was supported by the German Aerospace Center, DLR, under grant 50 QL 0001. We thank the NOAA Space Environment Center for free access to SXI data. Hα data were provided by the high-speed Hα imaging system at Kanzelhöhe Solar Observatory (a joint project of Kanzelhöhe and the Astrophysikalisches Institut Potsdam). Additional Hα and He I data were provided by the High Altitude Observatory of the National Center for Atmospheric Research, which is sponsored by the National Science Foundation, and by Big Bear Solar Observatory, New Jersey Institute of Technology. The authors are grateful to the *RHESSI* team (PI: R. P. Lin) for free access to data and the development of the software. *SOHO* is a joint mission of ESA and NASA.

REFERENCES

Biesecker, D. A., Myers, D. C., Thompson, B. J., Hammer, D. M., & Vourlidas, A. 2002, ApJ, 569, 1009
Brueckner, G. E., et al. 1995, Sol. Phys., 162, 357
Chen, P. F., Wu, S. T., Shibata, K., & Fang, C. 2002, ApJ, 572, L99
Delaboudinière, J.-P., et al. 1995, Sol. Phys., 162, 291
Delannée, C. 2000, ApJ, 545, 512
Gilbert, H. R., Holzer, T. E., Thompson, B. J., & Burkepile, J. T. 2004, ApJ, 607, 540
Gopalswamy, N., Kaiser, M. L., Sato, J., & Pick, M. 2000, in ASP Conf. Ser. 206, High Energy Solar Physics: Anticipating *HESSI*, ed. R. Ramaty & N. Mandzhavidze (San Francisco: ASP), 351
Khan, J. I., & Aurass, H. 2002, A&A, 383, 1018
Klassen, A., Aurass, H., Mann, G., & Thompson, B. J. 2000, A&AS, 141, 357
Lemen, J. R., et al. 2004, Proc. SPIE, 5171, 65
Lin, R. P., et al. 2002, Sol. Phys., 210, 3
Mann, G. 1995a, in Lecture Notes in Physics, 444, Coronal Magnetic Energy Releases, ed. A. O. Benz & A. Krüger (Berlin: Springer), 183
———. 1995b, J. Plasma Phys., 53, 109
Moreton, G. E. 1960, AJ, 65, 494
Narukage, N., Hudson, H. S., Morimoto, T., Akiyama, S., Kitai, R., Kurokawa, H., & Shibata, K. 2002, ApJ, 572, L109
Okamoto, T. J., Nakai, H., Keiyama, A., Narukage, N., UeNo, S., Kitai, R., Kurokawa, H., & Shibata, K. 2004, ApJ, 608, 1124
Thompson, B. J., Plunkett, S. P., Gurman, J. B., Newmark, J. S., St. Cyr, O. C., & Michels, D. J. 1998, Geophys. Res. Lett., 25, 2465
Thompson, B. J., Reynolds, B., Aurass, H., Gopalswamy, N., Gurman, J. B., Hudson, H. S., Martin, S. F., & St. Cyr, O. C. 2000, Sol. Phys., 193, 161
Tsuneta, S., et al. 1991, Sol. Phys., 136, 37
Uchida, Y. 1974, Sol. Phys., 39, 431
Vršnak, B., Warmuth, A., Brajša, R., & Hanslmeier, A. 2002, A&A, 394, 299
Warmuth, A., & Mann, G. 2005, A&A, 435, 1123
Warmuth, A., Vršnak, B., Aurass, H., & Hanslmeier, A. 2001, ApJ, 560, L105
Warmuth, A., Vršnak, B., Magdalenić, J., Hanslmeier, A., & Otruba, W. 2004a, A&A, 418, 1101
———. 2004b, A&A, 418, 1117
Zhukov, A. N., & Auchère, F. 2004, A&A, 427, 705